Particle-particle particle-mesh method for dipolar interactions: On error estimates and efficiency of schemes with analytical differentiation and mesh interlacing

Joan J. Cerdà,[1,a)] V. Ballenegger,[2] and C. Holm[3]
[1]*Instituto de Física Interdisciplinar y Sistemas Complejos, IFISC (CSIC-UIB), Universitat de les Illes Balears, E-07122 Palma de Mallorca, Spain*
[2]*Institut UTINAM, Université de Franche-Comté, CNRS, 16, route de Gray, 25030 Besançon Cedex, France*
[3]*Institute for Computational Physics, Universität Stuttgart, 70569 Stuttgart, Germany*

(Received 5 August 2011; accepted 11 October 2011; published online 14 November 2011)

The interlaced and non-interlaced versions of the dipolar particle-particle particle-mesh (P^3M) method implemented using the analytic differentiation scheme (AD-P^3M) are presented together with their respective error estimates for the calculation of the forces, torques, and energies. Expressions for the optimized lattice Green functions, and for the Madelung self-forces, self-torques and self-energies are given. The applicability of the theoretical error estimates are thoroughly tested and confirmed in several numerical examples. Our results show that the accuracy of the calculations can be improved substantially when the approximate (mesh computed) Madelung self-interactions are subtracted. Furthermore, we show that the interlaced dipolar AD-P^3M method delivers a significantly higher accuracy (which corresponds approximately to using a twice finer mesh) than the conventional method, allowing thereby to reduce the mesh size with respect to the non-interlaced version for a given accuracy. In addition, we present similar expressions for the dipolar ik-differentiation interlaced scheme, and we perform a comparison with the AD interlaced scheme. Rough tests for the relative speed of the dipolar P^3M method using ik-differentiation and the interlaced/non-interlaced AD schemes show that when FFT computing time is the bottleneck, usually when working at high precisions, the interlaced AD-scheme can be several times faster than the other two schemes. For calculations with a low accuracy requirement, the interlaced version can perform worse than the ik and the non-interlaced AD schemes. © *2011 American Institute of Physics*. [doi:10.1063/1.3657407]

I. INTRODUCTION

Dipole-dipole interactions are important in many soft-matter systems ranging from dispersions of magnetic micro and nanoparticles (ferrofluids) and electro-rheological fluids to magnetic thin films and water.[1–6] In numerical simulations, periodic boundary conditions are frequently used in order to approach bulk systems within the limits of currently available computers (see Ref. 7 for a detailed discussion about the adequacy of such methods to describe electrostatic systems). If a system of N particles with positions $\{\boldsymbol{r}_i\}$ $(i = 1, \ldots, N)$ in a cubic box of length L that carry point dipoles $\{\boldsymbol{\mu}_i\}$ is considered, then the total electrostatic energy under periodic boundary conditions is given, in Gaussian units, by

$$U = \frac{1}{2}\sum_{i=1}^{N}\sum_{j=1}^{N}{\sum_{\boldsymbol{n}\in\mathbb{Z}^3}}' v(\boldsymbol{r}_{ij} + \boldsymbol{n}L, \boldsymbol{\mu}_i, \boldsymbol{\mu}_j),$$

where $\boldsymbol{r}_{ij} = \boldsymbol{r}_i - \boldsymbol{r}_j$, and

$$v(\boldsymbol{r}_{ij}, \boldsymbol{\mu}_i, \boldsymbol{\mu}_j) \equiv (\boldsymbol{\mu}_i \cdot \nabla_{\boldsymbol{r}_i})(\boldsymbol{\mu}_j \cdot \nabla_{\boldsymbol{r}_j})\frac{1}{|\boldsymbol{r}_{ij}|} \tag{1}$$

is the dipolar interaction. The innermost sum runs over all periodic images of the system, identified by the shifting integer vector $\boldsymbol{n}$. The prime in the sum indicates that the $i = j$ term must be omitted for $\boldsymbol{n} = 0$. Note that the dipolar sum is conditionally convergent, so its value depends on the summation order. In the following, we assume that the sum is performed over spherical shells.

Advanced algorithms have been proposed to speed up the calculation of dipolar interactions in periodic boundary conditions: the dipolar Ewald sum,[8,9] the dipolar Lekner sum,[6] dipolar particle-mesh Ewald methods, such as smooth particle-mesh Ewald (SPME)[10] and particle-particle particle-mesh (P^3M),[11] and multipole Methods.[12–15] For a general overview of these algorithms, see the reviews in Refs. 6 and 16.

The particle-mesh Ewald methods take advantage of the fast Fourier transform (FFT) to accelerate the computation of the Fourier contribution to the Ewald sum. They scale as $\mathcal{O}(N \log N)$, i.e., almost linearly with the number of particles, and turn out to be the fastest method for systems of moderate size ($300 \lesssim N \lesssim 100\,000$).[17,18] Several variants of particle-mesh Ewald methods exist, that vary by different choices for specific ingredients in the method, such as the expression of the lattice Green function and the differentiation scheme used to compute forces from the electrostatic potential. The SPME and P^3M methods are compared in Refs. 18–20 (the last reference gives the exact mathematical link between the two methods). A key ingredient in the P^3M approach is that the lattice Green function is adjusted so as to make the root-mean-square (rms) error of the mesh calculation with respect to the exact continuous-space result as small as possible.[21] This ensures

a)Electronic mail: joan@ifisc.uib-csic.es.

that the P^{3}M method always provides the highest achievable accuracy for any given mesh size, assignment order (also known as spline interpolation order), differentiation scheme, etc. The optimization of the lattice Green function in the P^{3}M method also provides, as a by-product, an *a priori* error estimate for the method. The existence of such an error estimate is highly valuable because the accuracy depends strongly on the values chosen for the parameters of the method: Ewald splitting parameter, real-space cutoff, mesh size, and assignment order. The error estimate allows to find quickly parameter sets that achieve a given target accuracy for the forces, and the optimal set, i.e., the one that leads to the fastest computation, can then be determined from timings of force calculations performed with the few pre-selected parameter sets. Thanks to the *a priori* error estimate, this way of determining optimal parameters is fast and can entirely be automated, making the method easy to use: the only user-chosen parameter can be the accuracy of the calculation and thanks to the automatic tuning, optimal parameters will be chosen for the particular system under study (density of particles and strengths of dipoles).

In particle-mesh methods, the Poisson equation is solved on a mesh in Fourier space, via multiplication of the FFT of the charge density by a lattice Green function, and forces are obtained by computing the gradient of the potential energy of the particles. This energy gradient (and the "dipolar" gradients that appear in the dipolar interaction (1)) can be computed either in Fourier space by multiplying the potential by $i\boldsymbol{k}$ (the so-called $i\boldsymbol{k}$-differentiation scheme, also known as force-interpolation scheme), or in real space by using finite differences (FD-differentiation scheme) or by using the exact gradient of the function used to assign charges or dipoles onto/from the mesh (analytic differentiation (AD) scheme). The $i\boldsymbol{k}$-differentiation scheme has the advantage of being the most accurate one and to conserve momentum exactly. But $i\boldsymbol{k}$-differentiation is computationally expensive, as it requires three inverse three-dimensional (3D) FFTs to transform the vectorial electrostatic field mesh back to real space, whereas a single 3D-FFT is needed to transform back the scalar electrostatic potential mesh when using analytic differentiation. The AD scheme was introduced already in the 1970s (see Ref. 22 and references therein), but it was brought into widespread use only 25 years later as an ingredient in the SPME method.[23]

In the generalization of the SPME method to dipolar interactions, several variants of the method have been introduced, depending on how the gradients are computed.[10] These variants are called dipolar SPME (all gradients are computed analytically in real space), PME-FI (mixed scheme where "dipolar" gradients are computed analytically, while the energy gradient is computed in Fourier space) and PME-FII (all gradients are computed in Fourier space). The number of Fourier transforms required by these three methods to compute the forces and torques are, respectively, 2, 4, and 9 for purely dipolar systems (more Fourier transforms are needed in the case of charge/dipole mixtures (see Ref. 10)). However, for all these methods, no *a priori* error estimate has been given and the lattice Green function is not optimized specifically for the dipolar interactions.

In Ref. 11, we optimized the lattice Green function of the dipolar P^{3}M method in the case of the i$\boldsymbol{k}$-differentiation scheme and provided error estimates for that dipolar ik-P^{3}M method. Note that it differs numerically from the PME-FII method by the use of the associated optimal dipolar P^{3}M lattice Green function and by the fact that *a priori* error estimates for the forces, torques, and energy are available. Since that method requires nine 3D-FFTs to compute forces and torques, while only two 3D-FFTs are needed when using the analytical differentiation scheme, the question of whether the use of the AD scheme can be more efficient in this context naturally arises. In the present work, we optimize the lattice Green function of the dipolar P^{3}M method in the case where the analytical differentiation is used, and derive the error estimates for the resulting dipolar AD-P^{3}M method. We assess then how that method performs in comparison to dipolar ik-P^{3}M, tuning the parameters of both methods to the same accuracy. It should be realized that the use of AD scheme does not necessarily lead to a faster algorithm, even if it requires less FFTs, because it provides significantly less accurate forces than the $i\boldsymbol{k}$-scheme for a given mesh size and assignment order. The AD scheme has furthermore the drawback that particles are subjected to self-forces, and that the pair interactions do not obey Newton's third law exactly, so that a correction to all forces must be introduced to conserve at least the center-of-mass momentum. That correction has the unfortunate collateral effect of breaking the exact conservation of energy that would otherwise hold for the AD scheme in the limit of small time steps (see discussion of energy-conserving schemes in Hockney and Eastwood's book[24]). In this paper, we provide also explicit analytical formulas for the self-forces and self-torques, as a function of the position of a dipole in a mesh cell that appear when using the AD scheme. These formulas can be used to subtract these spurious self-interactions within the particle-mesh calculation, thereby improving the accuracy of the method and the conservation of momentum. The analogous explicit formula for the self-energy of a dipole is also given, and can be used to correct, at the level of each particle, the approximate Madelung self-energies that are included in the mesh calculation. Since often only the total energy of the system is monitored, a simpler formula for correcting solely the bias of the *total* energy is moreover provided. The subtraction of self-interactions improves the accuracy of the mesh calculation in some region of the parameter space of the method (see Table I and discussion in Ref. 25).

Another ingredient that might enhance the efficiency of particle-mesh methods is mesh interlacing (or staggering). In the simplest implementation of interlacing, the mesh calculation is performed twice, the second time with a mesh shifted by a vector $\boldsymbol{p} = h/2(1, 1, 1)$ where h is the mesh spacing (i.e., it is shifted by half the diagonal of a mesh cell), and the average of the two mesh calculations is computed. If $\boldsymbol{T}$ is an observable at a point (for instance force, torque or energy) that depends on the configuration $\{\boldsymbol{r}_i, \boldsymbol{\mu}_i\}_{i=1}^N$ of the system, it is computed in an interlaced P^{3}M algorithm as

$$\boldsymbol{T}^{(\text{interlaced})} = \frac{\boldsymbol{T}(\{\boldsymbol{r}_i, \boldsymbol{\mu}_i\}_{i=1}^N) + \boldsymbol{T}(\{\boldsymbol{r}_i + \boldsymbol{p}, \boldsymbol{\mu}_i\}_{i=1}^N)}{2}. \quad (2)$$

(A computationally cheaper way of implementing interlacing is to average structure factors instead of forces as explained in Ref. 24). The idea of interlacing was introduced long ago by Chen and Langdon[26] and is explained in details in Ref. 24, but it had been almost forgotten until recently, when it has been applied to the SPME and P^{3}M algorithms for computing Coulomb interactions between point charges.[27,28] It has been found for charges that a P^{3}M method with interlacing provides the same accuracy as a conventional P^{3}M method with a twice finer mesh (the interlaced SPME method does not show such a high increase in accuracy when using interlacing). Mesh interlacing provides this accuracy gain by roughly doubling the cost of the mesh calculation, while doubling the mesh size in the conventional method would increase the cost of the FFTs by a factor 8. Interlacing can, thus, be competitive if it allows to reach the target accuracy using a significantly coarser mesh. In this paper, we provide also the optimal P^{3}M lattice Green function for the interlaced dipolar AD-P^{3}M algorithm, together with the *a priori* error estimate of that method. The interlaced version of the dipolar AD-P^{3}M method is also included in our comparison of relative efficiencies of the different dipolar P^{3}M variants.

The outline of this paper is as follows. The basic formulas for the Ewald summation of dipolar interactions are recalled in Sec. II A. In Sec. II B, the non-interlaced and the interlaced dipolar P^{3}M algorithms using analytical differentiation scheme are presented, and the formulas for the Madelung-self force, torque, and energy needed to improve the accuracy of the calculations are presented. Theoretical estimates for the rms error of forces, torques, and energy, for the interlaced and non-interlaced dipolar AD-P^{3}M methods are presented in Sec. III. Numerical tests of the accuracy of the error estimates are provided in Sec. IV together with a comparison of the relative computing times for the ik-differentiation and the interlaced and non-interlaced AD schemes as a function of the required accuracy. That comparison should help to answer the question which is the preferable computation scheme under various circumstances. Technical details about dipolar P^{3}M using the analytical differentiation scheme, and the derivation of the Madelung-self forces and torques are given in the Appendix.

II. THE DIPOLAR AD-P^{3}M METHOD

The dipolar AD-P^{3}M method differs from the dipolar ik-P^{3}M method presented in Ref. 11 (hereafter referred to as paper I) by its use of the analytical differentiation scheme. Changing the differentiation schemes implies modifying the way the forces are computed in the algorithm, switching to the lattice Green function optimized for the AD scheme, and getting rid of unwanted self-interactions associated with the AD scheme by subtracting them within the particle-mesh calculation. These modifications are explained in Secs. II B and II C, using the same notations as in paper I. In Sec. II A, we recall briefly the dipolar Ewald summation, in which the method has its roots, to introduce some needed quantities. As in paper I, symbols $\check{f}(\boldsymbol{k})$, $\hat{f}(\boldsymbol{k})$, and $\widetilde{f}(\boldsymbol{k})$ denote a Fourier harmonic obtained, respectively, from a continuous Fourier transform, a Fourier series, and a discrete Fourier transform of function $f(\boldsymbol{r})$. We assume that the simulation box is cubic, but the generalization to triclinic boxes is straightforward (see for instance Refs. 10 and 20).

A. Ewald summation with dipolar interactions

The fundamental idea of the Ewald summation (and its advanced implementations such as the particle-mesh methods SPME and P^{3}M) is to calculate energies, forces, and torques in a system of N particles with positions $\{\boldsymbol{r}_i\}_{i=1}^{i=N}$ in a cubic box of length L that carry point dipoles $\{\boldsymbol{\mu}_i\}_{i=1}^{i=N}$ by splitting the long-ranged dipolar pair-interaction into two parts

$$v(\boldsymbol{r}, \boldsymbol{\mu}_i, \boldsymbol{\mu}_j) = (\boldsymbol{\mu}_i \cdot \nabla_{\boldsymbol{r}_i})(\boldsymbol{\mu}_j \cdot \nabla_{\boldsymbol{r}_j})(\psi(\boldsymbol{r}_{ij}) + \phi(\boldsymbol{r}_{ij})), \tag{3}$$

where $\psi(\boldsymbol{r})$ contains the short-distance part of the Coulomb interaction, and $\phi(\boldsymbol{r})$ contains its long-distance part ($\phi(\boldsymbol{r})$ must, moreover, be smooth everywhere and regular at the origin). The standard way to perform this splitting is to set

$$\psi(r) \equiv \frac{\operatorname{erfc}(\alpha r)}{r}, \qquad r = |\boldsymbol{r}|, \tag{4}$$

$$\phi(r) \equiv \frac{\operatorname{erf}(\alpha r)}{r}, \tag{5}$$

though other choices are possible.[29–32] The inverse length α, which is often referred to as the Ewald (or splitting) parameter, weighs the importance of one term with respect to the other, and can be chosen so as to optimize the performance. The interactions associated with the function ψ are short-ranged and they can, hence, efficiently be summed directly. The interactions associated with the function ϕ are long-ranged in real space, but short-ranged in the reciprocal Fourier space, and can, therefore, be efficiently computed in that latter space. The decomposition of the potential leads to the well-known Ewald formula for the electrostatic energy of a system of dipoles (see details in Refs. 6 and 33–35)

$$U = U^{(r)} + U^{(k)} + U^{(\mathrm{self})} + U^{(\mathrm{surf})}, \tag{6}$$

where the real-space energy $U^{(\mathbf{r})}$, the reciprocal-space energy $U^{(k)}$, the self-energy $U^{(\mathrm{self})}$, and the surface $U^{(\mathrm{surf})}$ contributions are

$$U^{(r)} = \frac{1}{2}\sum_{i,j=1}^{N}{\sum_{\boldsymbol{n}\in\mathbb{Z}^3}}'(\boldsymbol{\mu}_i \cdot \nabla_{\boldsymbol{r}_i})(\boldsymbol{\mu}_j \cdot \nabla_{\boldsymbol{r}_j})\psi(\boldsymbol{r}_{ij}), \tag{7}$$

$$U^{(k)} = \frac{1}{2V}\sum_{\substack{\boldsymbol{k}\neq 0\\ \boldsymbol{k}\in\mathbb{K}^3}} |\hat{\boldsymbol{\rho}}(\boldsymbol{k}) \cdot i\boldsymbol{k}|^2 \check{\phi}(\boldsymbol{k}), \tag{8}$$

$$U^{(\mathrm{self})} = -\frac{2\alpha^3}{3\sqrt{\pi}}\sum_{i=1}^{N}\boldsymbol{\mu}_i^2, \tag{9}$$

$$U^{(\mathrm{surf})} = \frac{2\pi}{(2\epsilon'+1)V}\sum_{i=1}^{N}\sum_{j=1}^{N}\boldsymbol{\mu}_i \cdot \boldsymbol{\mu}_j, \tag{10}$$

where $V = L^3$ is the volume of the box, and ϵ' is the dielectric constant of the medium surrounding the replica boxes:

$\epsilon' = 1$ for vacuum, and $\epsilon' = \infty$ for metallic boundary conditions. Because of the periodic boundary conditions, wave vectors $\boldsymbol{k} \in \mathbb{K}^3$ are discrete where $\mathbb{K}^3 \equiv \{2\pi \boldsymbol{n}/L : \boldsymbol{n} \in \mathbb{Z}^3\}$. In Eq. (8), $\hat{\boldsymbol{\rho}}(\boldsymbol{k})$ is the Fourier transform of the periodic dipole density,

$$\boldsymbol{\rho}(\boldsymbol{r}) = \sum_{i=1}^{N} \boldsymbol{\mu}_i \, \delta(\boldsymbol{r} - \boldsymbol{r}_i), \qquad \boldsymbol{r} \in V, \tag{11}$$

which reads

$$\hat{\boldsymbol{\rho}}(\boldsymbol{k}) \equiv \mathrm{FT}[\boldsymbol{\rho}](\boldsymbol{k}) = \sum_{i=1}^{N} \boldsymbol{\mu}_i \, e^{-i\boldsymbol{k}\cdot\boldsymbol{r}_i}. \tag{12}$$

In Eq. (8), the Fourier transform $\breve{\phi}(\boldsymbol{k})$ of the reciprocal interaction (5) is

$$\breve{\phi}(\boldsymbol{k}) = \int \phi(\boldsymbol{r}) e^{-i\boldsymbol{k}\cdot\boldsymbol{r}} \mathrm{d}\boldsymbol{r} = \frac{4\pi}{k^2} e^{-k^2/4\alpha^2}. \tag{13}$$

The term $U^{(\mathrm{self})}$ subtracts the unwanted Ewald self-energies that are included in the reciprocal energy $U^{(k)}$, where the Ewald self-energy of a dipole is defined as the reciprocal interaction of the dipole with itself: $\lim_{\boldsymbol{r}\to 0}(-\frac{1}{2}) \left(\boldsymbol{\mu}_i \cdot \nabla_{\boldsymbol{r}}\right)^2 \phi(\boldsymbol{r})$.

It should be remarked that the expression given in Eq. (10) for the surface term is valid only when a spherical order of summation is used in the calculation of the direct sum.[34,35] That term vanishes, if metallic boundary conditions ($\epsilon' = \infty$) are used.

Ewald expressions for the force and electric field acting on a dipole i follow from the expressions $\boldsymbol{F}_i = -\nabla_{\boldsymbol{r}_i} U$, $\boldsymbol{E}_i = -\nabla_{\boldsymbol{\mu}_i} U$, and Eq. (6),

$$\boldsymbol{F}_i = \boldsymbol{F}_i^{(r)} + \boldsymbol{F}_i^{(k)}, \tag{14}$$

$$\boldsymbol{E}_i = \boldsymbol{E}_i^{(r)} + \boldsymbol{E}_i^{(k)} + \boldsymbol{E}_i^{(\mathrm{self})} + \boldsymbol{E}_i^{(\mathrm{surf})}, \tag{15}$$

where the superscripts (r) and (k) denote the real-space and reciprocal-space contributions. Notice that there is no self- nor surface-contribution to the force because the self- and surface-energy terms (Eqs. (9) and (10)) are independent of the particle positions. The torque on dipole i follows directly from the electric field: $\boldsymbol{\tau}_i = \boldsymbol{\mu}_i \times \boldsymbol{E}_i$. Notice that in electrostatics $\nabla \times \boldsymbol{E} = 0$, and therefore, forces can be computed using either $\boldsymbol{F}(\boldsymbol{r}) = \nabla_r(\boldsymbol{\mu} \cdot \boldsymbol{E}(\boldsymbol{r}))$ or $\boldsymbol{F}(\boldsymbol{r}) = (\boldsymbol{\mu} \cdot \nabla_r)\boldsymbol{E}(\boldsymbol{r})$. The reader is referred to Ref. 9 for fully explicit Ewald formulas for the real space and reciprocal space contributions to the force and torque.

B. Algorithmic details of the mesh calculations

When using P^{3}M , the computation of the real-space contribution $U^{(\mathbf{r})}$ is the same than for the Ewald formula.[9] In the following, we discuss in detail the mesh calculation in the case where the analytic differentiation (AD) scheme is used. The mesh calculation proceeds essentially in three steps: (1) Dipole assignment onto mesh points; (2) Solution of Poisson equation in Fourier space; (3) Fourier transformation back to real space, with derivation and interpolation of the mesh results onto the dipole positions in continuous space. Each step is performed slight differently than in the dipolar P^{3}M method with $i\boldsymbol{k}$-differentiation[11] because the gradients are now computed analytically by using the exact gradient of the assignment function instead of introducing the differential operator $\boldsymbol{D}(\boldsymbol{k}) \equiv i\boldsymbol{k}$ in Fourier space.

Let N_M be the number of mesh points in each direction, and $h = L/N_M$ be the lattice spacing. We denote by $\mathbb{M}^3$ the set of all points belonging to the mesh: $\mathbb{M}^3 \equiv \{nh : n \in \mathbb{Z}^3, 0 \le n_{x,y,z} < N_M\}$. An index "M" is attached to any quantity defined at mesh points only, e.g., the mesh-based electrostatic potential $\Phi_M(\boldsymbol{r}_m)$, $\boldsymbol{r}_{\boldsymbol{m}} \in \mathbb{M}^3$. The fast Fourier transform $\widetilde{f_M} = \mathrm{FFT}[f_M]$ of a mesh-based quantity yields the Fourier harmonics of this quantity in the "reciprocal mesh," which is defined as the set of wave vectors $\widetilde{\mathbb{M}}^3 \equiv \{2\pi \boldsymbol{n}/L : \boldsymbol{n} \in \mathbb{Z}^3, |n_{x,y,z}| < N_M/2\}$. The number of mesh points per direction N_M should preferably be a power of two, because in that case the FFTs are computed more efficiently.

1. Dipole assignment

A mesh mapped array of the dipoles $\rho_M(\boldsymbol{r}_m)$ is determined from the N dipolar particles $\{(\boldsymbol{r}_i, \boldsymbol{\mu}_i)\}$ by using the gradient of the usual P^{3}M *assignment function* $W(\mathbf{r})$ that maps the particles from their continuous positions onto the mesh

$$\rho_M(\boldsymbol{r}_m) = \frac{1}{h^3} \sum_{\substack{i=1 \\ m.i.c.}}^{N} \boldsymbol{\mu}_i \cdot \nabla_{\boldsymbol{r}_i} W(\boldsymbol{r}_m - \boldsymbol{r}_i), \tag{16}$$

where the minimum image convention (*m.i.c.*) is used when computing relative distances $\boldsymbol{r}_m - \boldsymbol{r}_i$. Notice that Eq. (16) is analogous to the formula used to define the charge array in the standard P^{3}M method for point charges, with the substitution $q_i \to \boldsymbol{\mu}_i \cdot \boldsymbol{\nabla}_i$.

We use the standard Hockney and Eastwood's assignment functions[24,36] $W(\boldsymbol{r})$, which are (shifted) B-splines and are tabulated in Ref. 19. The gradient of such functions can straightforwardly be obtained by simple differentiation of the expressions in Ref. 19. The assignment functions are classified according to the number P of nearest grid points per coordinate direction over which the dipole is distributed. The quantity P is referred to as the *assignment order* (this parameter corresponds to the spline interpolation order defined in SPME). A formal expression for Hockney and Eastwood's assignment functions is $W^{(P)}(\boldsymbol{r}) = W^{(P)}(x)W^{(P)}(y)W^{(P)}(z)$, where

$$W^{(P)}(x) = \underbrace{\left(\chi\left[\frac{-1}{2}, \frac{1}{2}\right] \star \ldots \star \chi\left[\frac{-1}{2}, \frac{1}{2}\right]\right)}_{P-\text{fold}-\text{convolution}} \left(\frac{x}{h}\right) \tag{17}$$

and $\chi[-1/2, 1/2]$ is the characteristic function, i.e., the function that is 1 within this interval and 0 outside.

2. Solving the Poisson equation

The reciprocal electrostatic energy and potential are computed at each mesh point $\boldsymbol{r}_m$ by approximating

Eq. (8) by

$$U_M^{(k)} = \frac{1}{2V} \sum_{\substack{\boldsymbol{k}\in\widetilde{\mathbb{M}}^3 \\ \boldsymbol{k}\neq\boldsymbol{0}}} \left|\widetilde{\boldsymbol{\rho}}_M(\boldsymbol{k})\right|^2 \widetilde{G}(\boldsymbol{k}), \tag{18}$$

$$\Phi_M^{(\boldsymbol{k})}(\boldsymbol{r}_m) = \mathrm{FFT}^{-1}_{\boldsymbol{k}\neq\boldsymbol{0}}\left[\widetilde{\Phi}_M^{(\boldsymbol{k})}\right](\boldsymbol{r}_m) = \frac{1}{L^3}\mathrm{FFT}^{-1}_{\boldsymbol{k}\neq\boldsymbol{0}}\left[\widetilde{\boldsymbol{\rho}}_M(\boldsymbol{k})\widetilde{G}(\boldsymbol{k})\right](\boldsymbol{r}_m). \tag{19}$$

Here, $\widetilde{\boldsymbol{\rho}}_M(\boldsymbol{k})$ is the fast Fourier transform of the mesh density $\rho_M(\mathbf{r})$. The $\boldsymbol{k} = 0$ term is excluded in the inverse transform FFT^{-1} of all mesh-based quantities as it is done in the reciprocal part of the Ewald sum. $\widetilde{G}(\boldsymbol{k})$ is the lattice Green function, also known as the *influence function*, and it is defined below, in Eq. (25).

3. Back interpolation

The mesh-based electrostatic potential is interpolated back to the particle positions $\boldsymbol{r}_i$ using the same assignment function $W(\boldsymbol{r})$ and the minimum image convention (*m.i.c.*):

$$\Phi^{(k)}(\boldsymbol{r}_i) = \sum_{\substack{\boldsymbol{r}_m\in\mathbb{M}^3 \\ m.i.c.}} \Phi_M^{(k)}(\boldsymbol{r}_m) W(\boldsymbol{r}_m - \boldsymbol{r}_i). \tag{20}$$

The electrostatic field can be obtained as follows:

$$\boldsymbol{E}^{(k)}(\boldsymbol{r}) = -\nabla_{\boldsymbol{r}}\Phi^{(k)}(\boldsymbol{r}) = -\sum_{\substack{\boldsymbol{r}_m\in\mathbb{M}^3 \\ m.i.c.}} \Phi_M^{(k)}(\boldsymbol{r}_m)\nabla_{\boldsymbol{r}} W(\boldsymbol{r}_m - \boldsymbol{r}). \tag{21}$$

Once the electric field is known, the forces and torques acting on a dipole $\boldsymbol{\mu}$ at point $\mathbf{r}$ are given by

$$\boldsymbol{F}^{(k)}(\boldsymbol{r}, \boldsymbol{\mu}) = \nabla_r(\boldsymbol{\mu}\cdot\boldsymbol{E}^{(k)}(\boldsymbol{r})), \tag{22}$$

$$\boldsymbol{\tau}^{(k)}(\boldsymbol{r}, \boldsymbol{\mu}) = \boldsymbol{\mu}\times\boldsymbol{E}^{(k)}(\boldsymbol{r}). \tag{23}$$

The gradient in Eq. (22) is computed using the second derivatives of the assignment function that appears in Eq. (21). Notice that, as mentioned in the Introduction, forces and torques are computed using only two FFTs when using the AD scheme, contrary to the *ik*-differentiation scheme which requires nine FFTs to compute dipole-dipole interactions.[11]

4. The lattice Green function

The optimal P^{3}M lattice Green function to compute dipolar interactions can be found by minimizing the rms error in the (reciprocal) pair interaction $\mathbf{T}^{(k)}$ between two unit dipoles in the simulation box

$$Q^2_{\mathrm{int}}[T^{(k)}] := \frac{1}{h^3(4\pi)^2 V}\int_{h^3} \mathrm{d}\boldsymbol{r}_1 \int_V \mathrm{d}\boldsymbol{r}_2 \int \mathrm{d}\boldsymbol{\Omega}_1 \int \mathrm{d}\boldsymbol{\Omega}_2 \times\left[\boldsymbol{T}^{(k)}(\boldsymbol{r}_1, \hat{\boldsymbol{\mu}}_1, \boldsymbol{r}_2, \hat{\boldsymbol{\mu}}_2) - \boldsymbol{T}^{(\mathrm{ex},k)}(\boldsymbol{r}_1, \hat{\boldsymbol{\mu}}_1, \boldsymbol{r}_2, \hat{\boldsymbol{\mu}}_2)\right]^2, \tag{24}$$

where $\boldsymbol{T}^{(\mathrm{ex},\,k)}(\boldsymbol{r}_1, \boldsymbol{\mu}_1, \boldsymbol{r}_2, \boldsymbol{\mu}_2)$ is the exact (reciprocal) dipolar Ewald interaction (energy, electrostatic field, force, or torque) between two dipoles, and $\mathbf{T}^{(k)}(\boldsymbol{r}_1, \boldsymbol{\mu}_1, \boldsymbol{r}_2, \boldsymbol{\mu}_2)$ is the P^{3}M pair interaction. The quantity Q^2_{int} defined in Eq. (24) is the squared error of the P^{3}M interaction averaged over all positions and orientations of the two dipoles in the simulation box. Notice that the average over $\mathbf{r}_1$ has been restricted to a single mesh cell h^3 thanks to the periodicity of the system.

The optimal influence function which results from the minimization of Eq. (24) for the AD scheme is found to be (see the Appendix for details and notations)

$$\widetilde{G}_{\mathrm{opt}}(\boldsymbol{k}) = \frac{\sum_{\boldsymbol{m}\in\mathbb{Z}^3}\left[[\boldsymbol{k}_{\boldsymbol{m}}]^{2S_1}\left(\breve{U}(\boldsymbol{k}_{\boldsymbol{m}})\right)^2\breve{\phi}(\boldsymbol{k}_{\boldsymbol{m}})\right]}{\sum_{\boldsymbol{m}\in\mathbb{Z}^3}[\boldsymbol{k}_{\boldsymbol{m}}]^{S_2}(\breve{U}(\boldsymbol{k}_{\boldsymbol{m}}))^2\sum_{\boldsymbol{n}\in\mathbb{Z}^3}[\boldsymbol{k}_{\boldsymbol{mn}}]^{S_3}(\breve{U}(\boldsymbol{k}_{\boldsymbol{mn}}))^2 C(\boldsymbol{n})}, \tag{25}$$

where exponents S_1, S_2, and S_3 are given later for each observable, and $\boldsymbol{k}_{\boldsymbol{m}} \equiv \boldsymbol{k} + (2\pi/h)\boldsymbol{m}$, $\boldsymbol{k}_{\boldsymbol{mn}} \equiv \boldsymbol{k}_{\boldsymbol{m}} + (2\pi/h)\boldsymbol{n}$, $\breve{U}(\boldsymbol{k}) \equiv \breve{W}(\boldsymbol{k})/h^3$, and $\breve{W}(\boldsymbol{k})$ is the Fourier transform of the assignment function defined in Eq. (17),

$$\breve{W}(\boldsymbol{k}) = h^3\left(\frac{\sin(\frac{1}{2}k_x h)\sin(\frac{1}{2}k_y h)\sin(\frac{1}{2}k_z h)}{(\frac{1}{2}k_x h)(\frac{1}{2}k_y h)(\frac{1}{2}k_z h)}\right)^P. \tag{26}$$

The function $C(\boldsymbol{n})$ is defined as

$$C(\boldsymbol{n}) \equiv \begin{cases} 1 & \text{non-interlaced variant,} \\ (1+\exp(i2\pi/h\boldsymbol{n}\cdot\boldsymbol{p}))/2 & \text{interlaced variant.} \end{cases} \tag{27}$$

Notice that $C(\boldsymbol{n}) \equiv (1 + \exp(i2\pi/h\boldsymbol{n}\cdot\boldsymbol{p}))/2$ reduces to $C(\boldsymbol{n}) = (1+(-1)^{n_x+n_y+n_z})/2$ when one uses the usual shift $\boldsymbol{p} = h/2(1, 1, 1)$ appropriate for interlacing with two meshes. In the interlaced variant, all terms where $n_x + n_y + n_z$ is odd drop out in the denominator of the optimal influence function (25). The influence function optimized for computing dipolar forces is obtained by setting ($S_1 = 3, S_2 = 2, S_3 = 4$). The values $S_1 = S_2 = S_3 = 2$ refer to the optimal influence function for the dipolar torques, energy, and the electrostatic field.

It should be remarked that the use of the different influence functions to compute the forces and torques does not imply any noticeable time overhead because influence functions are computed within seconds and stored at the beginning of the simulation, and they remain unaltered throughout the whole simulation. One can even use another remarkable fact, namely, in the limit of neglecting all aliasing sums over m, i.e., keeping only the $m = 0$ contribution, all optimal influence functions reduce to the same functional, given by Eq. (25) for $m = 0$, which also coincides with the optimal influence function for Coulomb energies and forces in that limit,

$$\widetilde{G}_{\mathrm{opt}}(\boldsymbol{k}) = \frac{\breve{\phi}(\boldsymbol{k})}{\breve{U}(\boldsymbol{k})^2}. \tag{28}$$

Moreover, the actual value of the exact influence functions for energies, forces, and torques is quite insensitive to the neglect of these terms, i.e., errors induced by this cutoff are very small. This would allow for using a single optimal influence function for all needed quantities. In general, this last approach will not result in a noticeable performance increase for simulations at constant volume because the influence functions are computed only once at the beginning of those simulations. However, in the case of constant pressure simulations where influence function must be recomputed each time the

volume of the box is changed,[11] this simplification is expected to increase the performance. We warn already the reader that if one wants to compute the errors accurately (see Sec. III) the use of the $m = 0$ approximation is not possible.

Another important aspect to take into account when implementing the method is that the reciprocal mesh must be symmetric (if wave vector k belongs to the mesh, so does $-k$) to avoid additional biases on the computed quantities. It is also worth to remark that in the non-interlaced case, the denominator in Eq. (25) can be decoupled as

$$\sum_{\boldsymbol{m}\in\mathbb{Z}^3} [\boldsymbol{k}_{\boldsymbol{m}}]^{S_2} (\breve{U}(\boldsymbol{k}_{\boldsymbol{m}}))^2 \sum_{\boldsymbol{a}\in\mathbb{Z}^3} [\boldsymbol{k}_{\boldsymbol{ma}}]^{S_3} (\breve{U}(\boldsymbol{k}_{\boldsymbol{ma}}))^2 = \left[\sum_{\boldsymbol{m}\in\mathbb{Z}^3} [\boldsymbol{k}_{\boldsymbol{m}}]^{S_2} (\breve{U}(\boldsymbol{k}_{\boldsymbol{m}}))^2\right]\left[\sum_{\boldsymbol{m}\in\mathbb{Z}^3} [\boldsymbol{k}_{\boldsymbol{m}}]^{S_3} (\breve{U}(\boldsymbol{k}_{\boldsymbol{m}}))^2\right], \tag{29}$$

which makes the initial calculation of the optimal $\widetilde{G}_{\mathrm{opt}}(\boldsymbol{k})$ even faster.

The influence functions (25) can be compared to those obtained when using the *ik-differentiation* scheme. The result for the *ik* non-interlaced scheme is already known (see Ref. 11), while for the interlaced *ik*-scheme, it is easy to prove, by following similar steps than in the AD-interlaced case, that the optimal influence function is

$$\widetilde{G}_{\mathrm{opt}}(\boldsymbol{k}) = \frac{\sum_{\boldsymbol{m}\in\mathbb{Z}^3}\left[\left[\widetilde{\boldsymbol{D}}(\boldsymbol{k})\cdot i\boldsymbol{k}_{\boldsymbol{m}}\right]^S (\breve{U}(\boldsymbol{k}_{\boldsymbol{m}}))^2 \breve{\phi}(\boldsymbol{k}_{\boldsymbol{m}})\right]}{\left[\widetilde{\boldsymbol{D}}(\boldsymbol{k})\right]^{2S} \sum_{\boldsymbol{m}\in\mathbb{Z}^3} \left(\breve{U}(\boldsymbol{k}_{\boldsymbol{m}})\right)^2 \sum_{\boldsymbol{n}\in\mathbb{Z}^3} \left(\breve{U}(\boldsymbol{k}_{\boldsymbol{mn}})\right)^2 C(\boldsymbol{n})}, \tag{30}$$

where $S = 3$ is used for the force, while $S = 2$ is used for the dipolar torques, energy, and the electrostatic field. Eqs. (25) and (30) differ only by the replacement of the $i\boldsymbol{k}_{\boldsymbol{m}}$ by the differential operator $\widetilde{\boldsymbol{D}}(\boldsymbol{k}) = i\boldsymbol{k}$. Notice that, in the *ik*-scheme, due to the periodicity of the differential operator, it has been possible in the denominator to extract the differential operators from inside the sums, while that is not possible in the AD-scheme where the non-periodic $i\boldsymbol{k}_{\boldsymbol{m}}$ is used. Similar replacements $i\boldsymbol{k}_{\boldsymbol{m}} \to \widetilde{\boldsymbol{D}}(\boldsymbol{k})$ will also appear when converting the expressions for the self-interactions and the error estimates of dipolar AD-P^{3}M to the ik-P^{3}M scheme. This small change in the formulas is, however, all what is needed to account for the changes in accuracy when switching between the two differentiation schemes either in the interlaced or non-interlaced variants.

As mentioned in the Introduction, an important by-product of the optimization of the lattice Green function is that it provides error estimates for the method, which are needed results when searching for optimal parameters for the method.

C. Madelung-Self interactions and correction term for the energy

By Madelung interaction, we mean the interaction of a particle (dipole) with its own periodic images. Madelung interactions can be considered as a special kind of self-interactions. "True" self-interactions (i.e., interaction of a particle with itself in the main cell) are also present in particle-mesh methods because self-interactions are naturally included when computing the interactions within an N-body system in Fourier space, and they are not entirely suppressed when subtracting the Ewald self-energy term (9) to the approximate mesh energy (18). By Madelung-self interaction (MS interaction), we mean the sum of the Madelung interaction and the true self-interaction (if any).

In paper I, we showed that, when using the *ik*-differentiation scheme, the MS force vanishes identically, while particles are subjected to a MS torque and a MS energy. Inaccuracies in the MS energies of the particles in the particle-mesh calculation give rise to a systematic bias in the computed energies, which can be removed by applying a simple correction to the P^{3}M energy. The existence of MS torques is not troublesome, because they average to zero (at least when the orientations of the dipolar particles are not correlated).

When using the AD scheme, there appears not only a MS energy and a MS torque, but also a MS force. As shown in the Appendix, the exact expressions for MS force, MS torque, and MS energy of a single particle are

$$\boldsymbol{F}^{(k)}_{\mathrm{MS}}(\boldsymbol{r},\boldsymbol{\mu}) = \frac{-i}{V}\sum_{\substack{\boldsymbol{k}\in\widetilde{\mathbb{M}}^3\\ \boldsymbol{k}\neq 0}} \widetilde{G}_{\mathrm{opt}}(\boldsymbol{k}) \sum_{\boldsymbol{m}\in\mathbb{Z}^3} \breve{U}(\boldsymbol{k}_{\boldsymbol{m}})(\boldsymbol{\mu}\cdot\boldsymbol{k}_{\boldsymbol{m}}) \sum_{\boldsymbol{n}\in\mathbb{Z}^3} \boldsymbol{k}_{\boldsymbol{mn}}(\boldsymbol{\mu}\cdot\boldsymbol{k}_{\boldsymbol{mn}})\eta(\boldsymbol{r},\boldsymbol{k},\boldsymbol{m},\boldsymbol{n}), \tag{31}$$

$$\boldsymbol{\tau}^{(k)}_{\mathrm{MS}}(\boldsymbol{r},\boldsymbol{\mu}) = \frac{-2}{V}\sum_{\substack{\boldsymbol{k}\in\widetilde{\mathbb{M}}^3\\ \boldsymbol{k}\neq 0}} \widetilde{G}_{\mathrm{opt}}(\boldsymbol{k}) \sum_{\boldsymbol{m}\in\mathbb{Z}^3} \breve{U}(\boldsymbol{k}_{\boldsymbol{m}})(\boldsymbol{\mu}\cdot\boldsymbol{k}_{\boldsymbol{m}}) \sum_{\boldsymbol{n}\in\mathbb{Z}^3} (\boldsymbol{\mu}\times\boldsymbol{k}_{\boldsymbol{mn}})\eta(\boldsymbol{r},\boldsymbol{k},\boldsymbol{m},\boldsymbol{n}), \tag{32}$$

$$U^{(k)}_{\mathrm{MS}}(\boldsymbol{r},\boldsymbol{\mu}) = \frac{1}{2V}\sum_{\substack{\boldsymbol{k}\in\widetilde{\mathbb{M}}^3\\ \boldsymbol{k}\neq 0}} \widetilde{G}_{\mathrm{opt}}(\boldsymbol{k}) \sum_{\boldsymbol{m}\in\mathbb{Z}^3} (\boldsymbol{\mu}\cdot\boldsymbol{k}_{\boldsymbol{m}})\breve{U}(\boldsymbol{k}_{\boldsymbol{m}}) \sum_{\boldsymbol{n}\in\mathbb{Z}^3} (\boldsymbol{\mu}\cdot\boldsymbol{k}_{\boldsymbol{mn}})\eta(\boldsymbol{r},\boldsymbol{k},\boldsymbol{m},\boldsymbol{n}), \tag{33}$$

where

$$\eta(\boldsymbol{r},\boldsymbol{k},\boldsymbol{m},\boldsymbol{n}) \equiv \breve{U}(\boldsymbol{k}_{\boldsymbol{mn}})\exp(i2\pi(\boldsymbol{n}\cdot\boldsymbol{r})/h)C(\boldsymbol{n}). \tag{34}$$

The complex part in previous expressions cancels out due to symmetry. These formulas are useful to subtract the unwanted MS interactions within the particle-mesh algorithm, as proposed in Ref. 20 in the case of point charges. These corrections can improve the accuracy, at the expense on an extra calculation that scales linearly with the number of particles in the system N. The self-forces depend only on the position of a particle relative to a mesh cell, and can be tabulated easily once for all at the beginning of the simulation (the convergence is fast and a few values of m are in fact required).

TABLE I. Change of rms errors for forces ΔF and torques $\Delta\tau$ depending on whether the Madelung-self (MS) interactions are subtracted within the particle-mesh calculation using Eqs. (31) and (32). The system considered is the same as in Figure 1. The mesh size has $N_M = 32$ points in each direction and the real space cutoff is $r_{\text{cut}} = 4$. The Ewald splitting parameter is tuned in each case to its optimal value.

	MS interactions	P = 3	P = 5	P = 7
$\log_{10}(\Delta F)$	Included	− 1.85	− 3.25	− 4.33
$\log_{10}(\Delta F)$	Subtracted	− 1.96	− 3.47	− 4.62
	Accuracy gain	12%	25%	12%
$\log_{10}(\Delta\tau)$	Included	− 2.66	− 4.10	− 5.26
$\log_{10}(\Delta\tau)$	Subtracted	− 2.81	− 4.34	− 5.50
	Accuracy gain	14%	27%	27%

Table I shows a comparison of the accuracy one can get by either performing or leaving out the subtraction of the MS interactions in the non-interlaced case.

The MS forces and MS torques average to zero, so they do not lead to a systematic bias, but only to fluctuations. As in the case of the *i**k*-differentiation scheme, the MS energies do not average to zero, and lead to a systematic bias, if they are not corrected. If only the total energy is monitored, it is advantageous to compute, at the beginning of the simulation, the average MS energy of a particle, i.e.,

$$\left\langle U_{\text{MS}}^{(k)}\right\rangle = \frac{\mu^2}{6V}\sum_{\substack{\boldsymbol{k}\in\widetilde{\mathbb{M}}^3\\ \boldsymbol{k}\neq 0}}\widetilde{G}_{\text{opt}}(\boldsymbol{k})\sum_{\boldsymbol{m}\in\mathbb{Z}^3}\boldsymbol{k}_{\boldsymbol{m}}^2\breve{U}(\boldsymbol{k}_{\boldsymbol{m}}), \tag{35}$$

multiply it by the number of particles in the system, and subtract this quantity from the computed P^{3}M energies. If correlations are not too strong, both approaches will coincide in the limit of many particles. In the second approach, the right formula for computing the corrected P^{3}M energy is formally the same as in Ref. 11, i.e.,

$$U_{\text{P3M}} = U^{(r)} + U_M^{(k)} + U^{(\text{self})} + U^{(\text{surf})} + \langle U^{(\text{corr})}\rangle, \tag{36}$$

where

$$\langle U^{(\text{corr})}\rangle = -M^2\langle U_{\text{MS}}^{(k)}(\boldsymbol{r},\hat{\boldsymbol{\mu}})\rangle - \frac{2\alpha^3}{3\sqrt{\pi}} + \frac{2\pi}{3L^3}, \tag{37}$$

and $M^2 \equiv \sum_{i=1}^N \boldsymbol{\mu}_i^2$. We note that the MS interactions are common to all particle-mesh methods, and are, thus, also present in the SPME algorithms.

III. ERROR ESTIMATES FOR THE DIPOLAR AD-P^{3}M ALGORITHM

In this section, *a priori* error estimates for the rms error of the forces, torques, and energy in the case of the dipolar P^{3}M algorithm using the analytic differentiation scheme are presented. The accuracy of the P^{3}M method depends on the chosen values for the parameters of the method: the Ewald splitting parameter α, the real-space cut-off distance r_{cut}, the mesh size N_M, and the assignment order P, as well as on the parameters of the system: the number of particles N, the box length L, and the sum over all squared dipole moments, M^2.

It is very useful to have formulas that are able to predict the error associated with a set of parameter values. Not only do such formulas enable the user to control the accuracy of the calculation, but also they allow for an automatic tuning of the algorithm, so that it can run at its optimal operation point, thus saving computer time.

A measure of the accuracy is given by the rms error defined by

$$\Delta T \equiv \left\langle \sqrt{\frac{1}{N}\sum_{i=1}^{N}(\boldsymbol{T}(i) - \boldsymbol{T}^{(\text{ex})}(i))^2}\right\rangle, \tag{38}$$

where $\boldsymbol{T}(i)$ is the value of $\boldsymbol{T}$ (for example, electrostatic field, force, torque, or energy) associated with particle i as obtained from the P^{3}M method, and $\boldsymbol{T}^{(\text{ex})}(i)$ is the exact value as defined by the direct summation formulas. The angular brackets denote an average over particle configurations. In Eq. (38), i is a short-hand notation for $(\boldsymbol{r}_i, \boldsymbol{\mu}_i)$.

In the case where the *total* electrostatic energy U is measured, the rms error is defined by

$$\Delta U \equiv \sqrt{\langle (U - U^{(\text{ex})})^2\rangle}, \tag{39}$$

where U is the corrected P^{3}M energy with the self-energy subtracted, and $U^{(\text{ex})}$ is the exact energy that one would get using, for instance, a direct sum calculation. The calculation is done under the assumption that the positions and orientations of the dipoles are distributed randomly. In a previous work [11] it was shown that rms error estimates for dipolar-P^{3}M when the *i**k*-*differentiation* scheme is used still accurately predict the errors for dipolar systems in which the dipoles are strongly correlated. Here, for the AD-scheme, we expect a similar behavior for correlated systems. For random systems, the average over configurations reduces to

$$\langle\cdots\rangle \equiv \frac{1}{V^N}\frac{1}{(4\pi)^N}\int\cdots\int\cdots \mathrm{d}1\ldots\mathrm{d}N, \tag{40}$$

where $\int\ldots\mathrm{d}i$ denotes the integration over all positions and orientations of particle i.

In expressions that follow for the error estimates, we assume that the Madelung-Self interactions has been removed from the calculated forces and torques. Therefore, the only contribution to the error that remains is due to the interaction of a particle i with a particle $j \neq i$ (including the images of particles j in the periodic replicas of the simulation box). This contribution is denoted by the subscript int.

A. Error in the dipolar forces

When MS-forces are subtracted for each particle using Eq. (31), the rms error estimate for dipolar forces is given by

$$(\Delta F)^2 \simeq (\Delta F^{(r)})^2 + \frac{M^4}{N}Q_{\text{int}}^2[F^{(k)}], \tag{41}$$

where $\Delta F^{(\mathbf{r})}$ is the real space error,[9]

$$\Delta F^{(r)} \simeq M^2\left(V\alpha^4 r_{\text{cut}}^9 N\right)^{-1/2} \times\left[\frac{13}{6}C_c^2 + \frac{2}{15}D_c^2 - \frac{13}{15}C_cD_c\right]^{1/2} e^{-\alpha^2 r_{\text{cut}}^2}, \tag{42}$$

$$C_c \equiv 4\alpha^4 r_{\rm cut}^4 + 6\alpha^2 r_{\rm cut}^2 + 3, \tag{43}$$

$$D_c \equiv 8\alpha^6 r_{\rm cut}^6 + 20\alpha^4 r_{\rm cut}^4 + 30\alpha^2 r_{\rm cut}^2 + 15, \tag{44}$$

and $Q_{\rm int}^2[F^{(k)}]$ is given by the general expression $Q_{\rm int}^2[T^{(k)}]$ in which the optimal influence function $\widetilde{G}_{\rm opt}(\boldsymbol{k})$ is used, namely,

$$Q_{\rm int}^2[T^{(k)}] = \frac{a}{9V^2} \sum_{\substack{\boldsymbol{k}\in\widetilde{\mathbb{M}}^3 \\ \boldsymbol{k}\neq\boldsymbol{0}}} \left\{ \sum_{\boldsymbol{m}\in\mathbb{Z}^3} |\boldsymbol{k_m}|^{2S} (\breve{\phi}(\boldsymbol{k_m}))^2 - \widetilde{G}_{\rm opt}(\boldsymbol{k}) \sum_{\boldsymbol{m}\in\mathbb{Z}^3} (\boldsymbol{k_m})^{2S} (\breve{U}(\boldsymbol{k_m}))^2 \breve{\phi}(\boldsymbol{k_m}) \right\}, \tag{45}$$

using the parameters $(S = 3,\ a = 1)$ for dipolar forces. The short-hand notation $\boldsymbol{k_m} \equiv \boldsymbol{k} + (2\pi/h)\boldsymbol{m}$ is used. Expression (45) is similar to the error estimate in the case of the $i\boldsymbol{k}$-differentiation scheme, apart from the substitution $\widetilde{\boldsymbol{D}}(k) \to i\boldsymbol{k_m}$. Expression (45) holds in both the interlaced and non-interlaced variants, provided the proper optimal influence function is used (Eqs. (25) and (27)). Also, notice that if one uses Eq. (30), with the aforementioned substitution $i\boldsymbol{k_m} \to \widetilde{\boldsymbol{D}}(\boldsymbol{k})$, one can get the error estimates for the interlaced $i\boldsymbol{k}$-differentiation scheme. It is worth mentioning that the approach of retaining only the $\boldsymbol{m} = 0$ term in Eq. (45) will lead to very poor estimates of the errors because in such case the exact values of $\mathbf{T}^{(k)}$ are not properly evaluated. Good error estimates are obtained if the aliasing sums over $\boldsymbol{m} = (m_x, m_y, m_z) \in \mathbb{Z}^3$ are computed up to $|m_\alpha| \leq 2$ at least.

B. Error in the torques

When MS-torques are subtracted using Eq. (32), the rms error estimate for dipolar torques is

$$(\Delta\tau)^2 \simeq (\Delta\tau^{(r)})^2 + \frac{M^4}{N} Q_{\rm int}^2[\boldsymbol{\tau}^{(k)}], \tag{46}$$

where the real-space contribution $\Delta\tau^{(\mathbf{r})}$ is

$$\Delta\tau^{(r)} \simeq M^2 (V\alpha^4 r_{\rm cut}^7 N)^{-1/2} \left[\frac{1}{2}B_c^2 + \frac{1}{5}C_c^2\right]^{1/2} e^{-\alpha^2 r_{\rm cut}^2}, \tag{47}$$

with $B_c \equiv 2\alpha^2 r_{\rm cut}^2 + 1$ and $Q_{\rm int}^2[\boldsymbol{\tau}^{(k)}]$ is given by Eq. (45) using $(S = 2, a = 2)$. The optimal influence function for torques must be used in this case when evaluating Eq. (45).

C. Error in the total energy

If the total energy is computed according to Eq. (36), the rms error estimate for the total energy is

$$(\Delta U)^2 \simeq (\Delta U^{(r)})^2 + 2M^4 Q_{\rm int}^2\left[U_{\rm nc}^{(k)}\right] + \left\langle \left(\Delta U_{\rm nc,MS}^{(k)}\right)^2 \right\rangle - \left(\langle U^{(\rm corr)}\rangle\right)^2, \tag{48}$$

where $Q_{\rm int}^2[U_{nc}^{(k)}]$ is given in Eq. (45) using $(S = 2,\ a = 1)$, and $U_{\rm nc}$ is the non-corrected energy [obtained by dropping $\langle U^{(\rm corr)}\rangle$ in Eq. (36)]. The optimal influence function for energies must be used in this case when evaluating Eq. (45). The real-space contribution $\Delta U^{(\mathbf{r})}$ is

$$\Delta U^{(r)} \simeq M^2 \left(V\alpha^4 r_{\rm cut}^7\right)^{-1/2} \times \left[\frac{1}{4}B_c^2 + \frac{1}{15}C_c^2 - \frac{1}{6}B_c C_c\right]^{1/2} e^{-\alpha^2 r_{\rm cut}^2}. \tag{49}$$

The reduction of the error due to the use of the energy correction term $(\langle U^{(\rm corr)}\rangle)^2$ can be computed straightforwardly from Eq. (37). Finally, the contribution to the error arising from the Madelung-self energy $\langle(\Delta U_{\rm nc,MS}^{(k)})^2\rangle$ is quite involved and computationally intensive and, thus, of little use for the purpose of tuning the algorithm to its optimal performance point. Nonetheless, it is shown in Sec. IV that a reasonable estimate of the error in the energy is obtained by dropping out the last two terms $\langle(\Delta U_{\rm nc,MS}^{(k)})^2\rangle$ and $-(\langle U^{(\rm corr)}\rangle)^2$ in Eq. (48) because both terms tend to mutually cancel out. The determination of the optimal performance point of the algorithm for the energy can be done in just a few seconds using this last approach. A derivation for $\langle(\Delta U_{\rm nc,MS}^{(k)})^2\rangle$ in the case of the AD-scheme can be done following similar steps than those for the ik-differentiation (see Appendix B of Ref. 11) but using the slightly modified expressions of the energy for the AD case.

IV. NUMERICAL TESTS

In this section, the reliability of the theoretical error estimates derived in Sec. III is tested. These *a priori* estimates will be compared to numerical errors obtained using Eq. (38) on configurations of a test system. The exact numerical values $\mathbf{T}^{(\rm ex)}(i)$ needed to use Eq. (38) (or Eq. (39) in the case of the total energy) are obtained by a well converged standard dipolar Ewald sum in which all quantities are computed with a degree of accuracy $\delta \leq 10^{-10}$. The dipolar-Ewald sum has been thoroughly tested previously against direct sum calculations to ensure its accuracy. The calculations of the error estimates have been done by truncating the aliasing sums over $\boldsymbol{m} = (m_x, m_y, m_z) \in \mathbb{Z}^3$ at $|m_\alpha| \leq 2$. All the quantities in this section are calculated using an arbitrary length unit $\mathcal{L}$ and dipole moment unit $\mathcal{M}$. Therefore, for instance, torques and torque errors are given in units of $\mathcal{M}^2/\mathcal{L}^3$, while forces are given in units of $\mathcal{M}^2/\mathcal{L}^4$. Hereby, the theoretical rms error estimates will be plotted as lines, whereas numerical rms errors will be depicted by circles.

The test systems consist of $N = 100$ particles with dipole moment of strength $\mu = 1$ randomly distributed in a cubic box of length $L = 10$. Figures 1–3 show the rms error for forces, torques, and energy as a function of the Ewald splitting parameter α for calculations using a mesh of $N_M = 32$ points per direction. The real-space cutoff parameter is set to $r_{\rm cut} = 4$ in all plots. In each figure, plots (a) and (b) are done using non-interlaced and interlaced versions of the dipolar P^{3}M method, respectively. From the top to the bottom, the order of the assignment function increases from $P = 3$ to $P = 5$ and $P = 7$. The MS contributions have been corrected using Eqs. (31)–(33) in order to subtract for each particle the

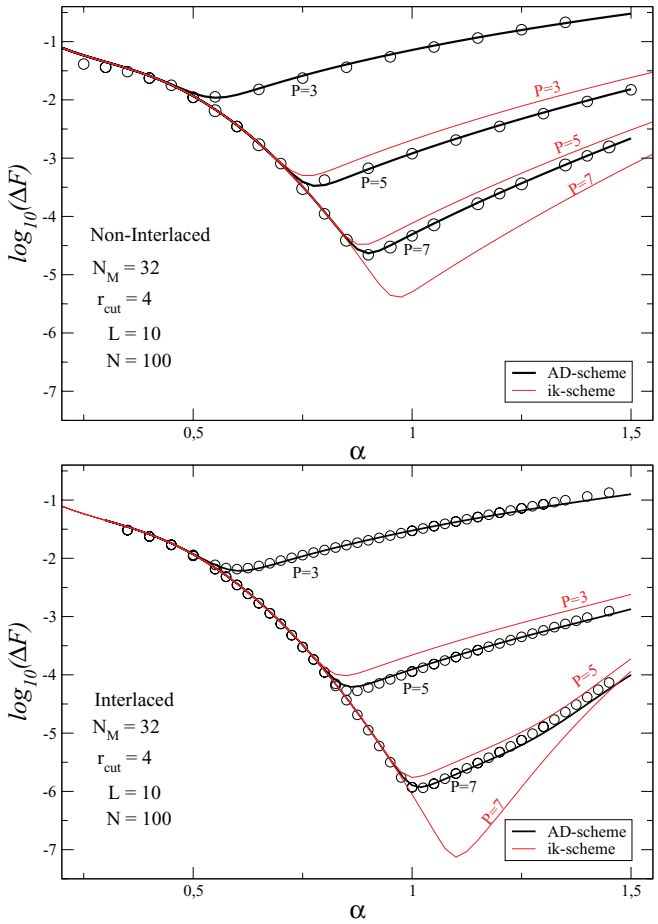

FIG. 1. RMS error ΔF of the forces (circles) using the AD-scheme for a system of 100 randomly distributed dipoles of strength $\boldsymbol{\mu} = 1$ in a box of size $L = 10$. The mesh has $N_M = 32$ points in each direction and the real space cutoff is $r_{\text{cut}} = 4$. From top to bottom, the order P of the assignment function is increased from 3 to 5 and 7. The solid black lines are the *a priori* error estimates for the AD-scheme (Eq. (41)). The solid red lines, are the error estimates when the ik-scheme is used (see discussion ca. Eqs. (30) and (45)). Plot (a) holds for the non-interlaced variant of the method, while plot (b) holds for the interlaced variant.

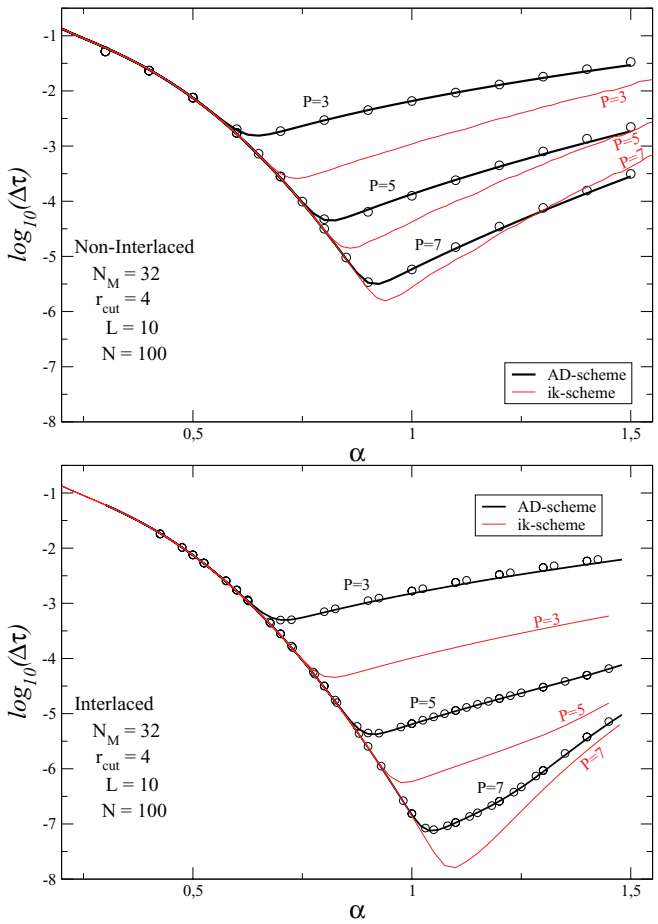

FIG. 2. Predicted and measured rms error of the torques $\Delta\tau$ for the same system as in Figure 1. Again, plot (a) holds for the non-interlaced variant, while plot (b) holds for the interlaced variant.

MS force, torque, and energy, respectively. Figure 1 shows, that the *a priori* rms error estimates for the force (Eq. (41)) give a good description of the rms errors in the whole range of values of the Ewald splitting parameter α. In comparison to the non-interlaced version, the accuracy of the interlaced algorithm is significantly higher (compare logarithmic plots 1(a) and 1(b)) thanks to the simple interlacing technique and to the introduction of the function $C(\boldsymbol{m})$ in the optimal influence function (see Eq. (25)). The observed increase in accuracy ranges between one and two orders of magnitude.

Figure 2 shows that for torques, the rms estimates, Eq. (46), give also a good description of the numerical rms error in the whole range of α's. Again, the use of interlacing leads to values about two orders of magnitude more accurate. Remarkably, when using the analytic differentiation scheme, the torques are calculated much more accurately than forces and energies.

Figure 3 shows a comparison of the theoretical error estimates for the total energy against the numerical rms error. The approximate theoretical rms estimate (dashed black lines) given by dropping the last two terms in Eq. (48), i.e.,

$$(\Delta U)^2 \simeq (\Delta U^{(r)})^2 + 2M^4 Q_{\text{int}}^2\left[U_{\text{nc}}^{(k)}\right], \tag{50}$$

predicts quite well the rms error for the energy, especially near the minimum of the curves, which are the regions of interest when tuning the method to its optimal operation point. This means that close to the minimum of the rms curves, the equality

$$\left\langle \left(\Delta U_{\text{nc,MS}}^{(k)}\right)^2 \right\rangle \simeq \left(\left\langle U^{(\text{corr})}\right\rangle\right)^2 \tag{51}$$

holds in good approximation. The big advantage of Eq. (50) compared to the exact result Eq. (48) is that it is much faster to compute Eq. (50) than Eq. (48). Therefore, it is suggested to use Eq. (50) in place of Eq. (48) to localize roughly the optimal performance point of the algorithm for the energies.

As expected, a comparison of the results using the non-interlaced AD scheme (black line in Figures 1(a), 2(a), and 3(a)) with those obtained for the same parameters but using the non-interlaced ik-scheme (red lines in the same figures), shows that, for the same set of parameters, the forces, torques, and energies are computed more accurately when ik-differentiation is used. This is specially marked in the case of forces, and in all cases where the assignment order P is low. But, as commented in the Introduction, the higher accuracy of the ik-scheme comes with the computational cost of seven

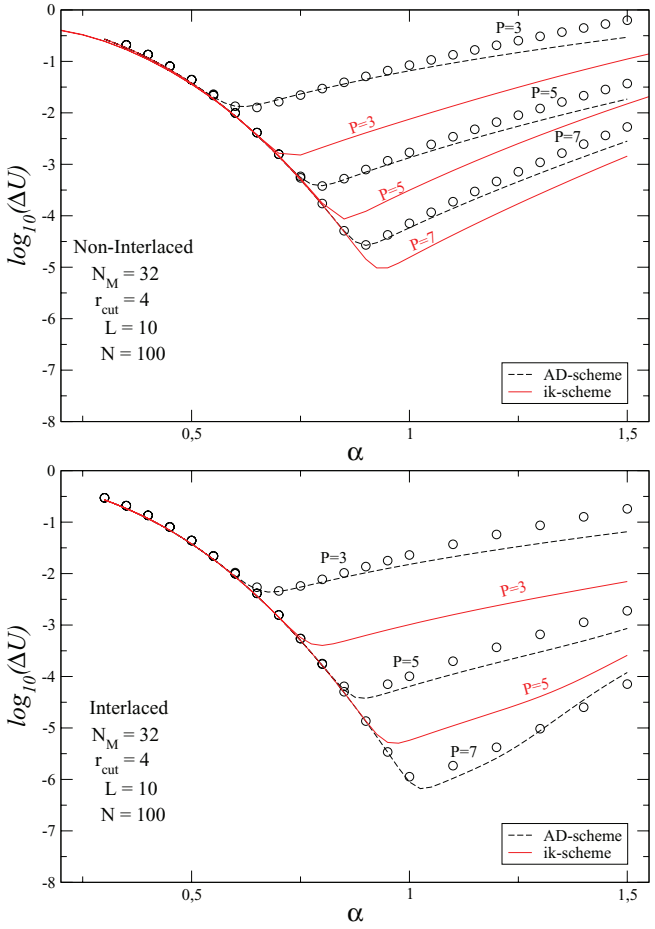

FIG. 3. Predicted and measured rms error of the total energy ΔU. In this case, the rms error has been obtained via Eq. (39) by averaging over 100 random configurations of the system. Again, plot (a) holds for the non-interlaced variant, while plot (b) holds for the interlaced variant. The dashed black lines represent the approximate error estimated obtained by dropping the last two terms in Eq. (48), i.e., using Eq. (50).

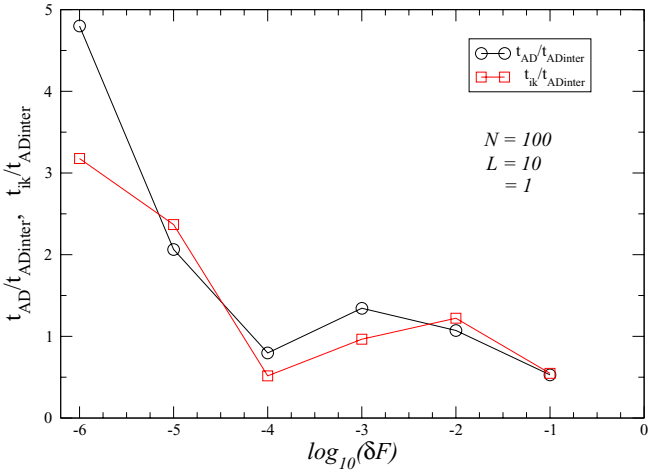

FIG. 4. Plot of relative computational times needed by three different methods (ik-P^{3}M, AD-P^{3}M, and interlaced AD-P^{3}M) to compute the dipolar interactions in a system of $N = 100$ particles with dipoles of strength $\boldsymbol{\mu} = 1$ in a cubic box of size $L = 10$. Circles show the relative speed of the AD-P^{3}M method with respect to interlaced AD-P^{3}M. Red squares show the relative speed of ik-P^{3}M with respect to interlaced AD-P^{3}M. In this rough estimation and for the given density of particles and value of dipoles, at high accuracies in the calculation of the force (i.e., $\delta F \sim 10^{-6}$), the interlaced AD-P^{3}M method is about five times faster than the non-interlaced version, and about three times faster than the ik-P^{3}M method. For low accuracy requirements ($\delta F \sim 10^{-1}$), non-interlaced ik-P^{3}M and AD-P^{3}M show quite similar speeds, and are about two times faster than the interlaced AD-P^{3}M.

additional 3D-FFTs. A similar increase in accuracy (in comparison to the non-interlaced AD-P^{3}M method) is obtained when using interlacing, at the expense of doubling roughly the computation time of the reciprocal space calculations. Thus, when momentum conservation is not crucial (e.g., in simulations using non-conserving momentum thermostats), the question emerges which of the methods (ik-scheme, AD non-interlaced, or interlaced) needs the least amount of CPU-time for a given accuracy.

A rough answer to this question can be inferred from Figure 4 where the relative speed of the ik-scheme (red squares) and the AD scheme (black circles), with respect to timings of the interlaced AD scheme, is provided, all algorithms being tuned to provide the same level of accuracy δF for the forces. Calculations have been done on a single CPU in a desktop computer (with two processors Intel(R)Core(TM)2 CPU 6600 at 2.40 GHz) using the FFTW3 library [37] to perform the FFT calculations. The considered system is the same as before (number of particles $N = 100$, cubic box of size $L = 10$, and dipole strength $\mu = 1$ in reduced units). Figure 4 shows that at low accuracies, the non-interlaced AD-P^{3}M method performs roughly twice faster than the interlaced AD-P^{3}M. This is because similar mesh sizes and assignment orders are required in both cases, only small changes in the real-space cutoff r_{cut} are needed to reach the accuracy goal, and therefore using the interlaced version amounts to perform twice the mesh calculations. This behavior reverses when a high accuracy is required; the non-interlaced scheme requires then a higher mesh size and/or assignment order, which makes the interlaced calculation more favorable. We observe moreover that, even though ik-P^{3}M requires more FFTs (9 versus 2), the calculation times turn out to be quite similar, at low accuracies, to those of non-interlaced AD-P^{3}M. The higher accuracy delivered by the ik-differentiation scheme allows to reduce the mesh size and/or the assignment order, which compensates (or even more than compensates) for the computational cost of the additional FFTs. The exact relative timings of the different methods depend on fine details, i.e., exact values of δF, N, L, and μ. For high accuracies, ik-P^{3}M is faster than AD-P^{3}M (compare the ratio of the two curves), but both methods are outperformed by the interlaced AD-P^{3}M. Among the considered schemes (ik or AD differentiation, interlacing), there is thus not a particular combination that is always the fastest, irrespective of the required accuracy.

Figure 5 shows that the conclusions inferred from Figure 4 are not modified qualitatively when systems with a larger number of N particles are simulated (all considered methods scale as $N\log(N)$). We increased the number of particles, while keeping the density fixed at $\rho = N/L^3 = 0.1$. The requested accuracy for all force calculations in Figure 5 is $\delta F \sim 10^{-4}$ (a typical accuracy requested in numerical simulations). In Figure 5, it can be observed that

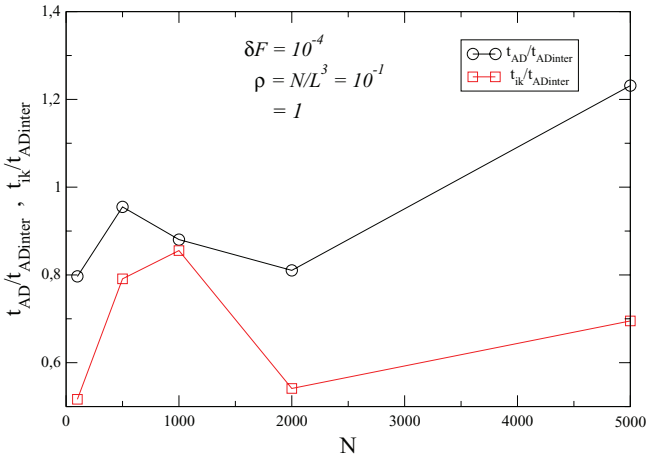

FIG. 5. The plot depicts, as in Figure 4, the relative times for the three different methods, but here the evolution of the relative times with the number of particles in the system is monitored. The accuracy is set to a constant value of $\delta F \sim 10^{-4}$, and the density is as in Figure 4 $\rho = N/L^3 = 0.1$. Colors and symbols have the same meaning as in Figure 4.

the relative times depend slightly on the value of N but qualitative aspects remain the same as in the case of $N = 100$.

V. CONCLUSIONS

In this work, an extension of the P^{3}M method of Hockney-Eastwood to the case of dipolar interactions using the analytic differentiation scheme has been presented. Both, interlaced and non-interlaced variants have been implemented and compared, and optimal influence functions for dipolar forces, torques, and energy have been derived. We have calculated expressions for the Madelung and self interaction terms arising from the use of the AD-scheme and it has been shown that the subtraction of those MS terms, which should be strictly zero, if the method was exact, leads to an improvement in the accuracy of the forces, torques, and energies. We obtained also, as by-products, accurate rms error estimates for the forces, torques, and energy. The validity of these estimates has been demonstrated numerically by computing the errors for test systems, using various parameter sets, and comparing them to our analytical estimates. Consequently, these formulas enable to determine the parameter combination that yields the optimal performance for a specified accuracy. This is conveniently done prior to running an actual simulation. Furthermore, our comparison of the interlaced and non-interlaced versions of dipolar AD-P^{3}M has shown that interlacing increases up to two orders of magnitude the accuracy of forces, torques, and energies.

In addition to the expressions for the AD-scheme, we have also presented the influence functions for the ik-P^{3}M interlaced scheme, and how one can easily from them derive the error estimates. We have observed that ik-P^{3}M always produces more accurate results than the AD scheme for both interlaced and non-interlaced variants. A comparison of the relative speed of AD schemes and of their relative speed compared to dipolar ik-P^{3}M has shown that the fastest method depends on the required level of accuracy. For calculations with a high-accuracy requirement, the interlaced AD-P^{3}M method introduced in this paper is the optimal choice, provided momentum non-conservation is not an issue. For calculations at low accuracies, the interlaced AD-P^{3}M method is the slowest among the three variants, while ik-P^{3}M and AD-P^{3}M show quite similar timings. Moreover, surprisingly the ik-P^{3}M seems to perform quite similar, or even slightly better, than the AD-P^{3}M despite its need for considerable more FFT operations.

ACKNOWLEDGMENTS

All authors are grateful to the DAAD organization for providing financial support. C.H. thanks the DFG for support through the SimTech center of excellence, the ScaFaCoS collaboration, and the SFB 716, and acknowledges helpful discussions with A. Arnold and M. Pippig.

APPENDIX: BUILDING UP THE DIPOLAR AD-P^{3}M ALGORITHM

1. The optimal influence function

In this Appendix, the analytical expressions for the optimal influence functions $\widetilde{G}$ are derived (see Eq. (25)), and the measure Q_{int} of the error for forces, torques, and the energy is provided (see Eq. (24)). The derivation is done in close analogy to paper I.[11]

The Parseval theorem for Fourier series

$$\int_V |f(\boldsymbol{r})|^2 \, \mathrm{d}\boldsymbol{r} = \frac{1}{V} \sum_{\boldsymbol{k} \in \widetilde{\mathbb{K}}^3} \left| \hat{f}(\boldsymbol{k}) \right|^2, \tag{A1}$$

allows to rewrite the measure of the error $Q^2[\boldsymbol{T}^{(k)}]$, Eq. (24), for a system containing two dipolar unit particles $(\boldsymbol{r}_1, \hat{\boldsymbol{\mu}}_1)$ and $(\boldsymbol{r}_2, \hat{\boldsymbol{\mu}}_2)$ as

$$Q^2_{\text{int}}[\boldsymbol{T}^{(k)}] = \frac{1}{(4\pi)^2 V^4} \sum_{\substack{\boldsymbol{k}_1 \in \widetilde{\mathbb{K}}^3 \\ \boldsymbol{k}_1 \neq \boldsymbol{0}}} \sum_{\substack{\boldsymbol{k}_2 \in \widetilde{\mathbb{K}}^3 \\ \boldsymbol{k}_2 \neq \boldsymbol{0}}} \int d\boldsymbol{\Omega}_1 \int d\boldsymbol{\Omega}_2$$

$$\times \left[|\hat{\boldsymbol{T}}^{(k)}(\boldsymbol{k}_1, \boldsymbol{k}_2, \hat{\boldsymbol{\mu}}_1, \hat{\boldsymbol{\mu}}_2)|^2 + |\hat{\boldsymbol{T}}^{(k,\text{ex})}(\boldsymbol{k}_1, \boldsymbol{k}_2, \hat{\boldsymbol{\mu}}_1, \hat{\boldsymbol{\mu}}_2)|^2 \; - 2\hat{\boldsymbol{T}}^{(k)}(\boldsymbol{k}_1, \boldsymbol{k}_2, \hat{\boldsymbol{\mu}}_1, \hat{\boldsymbol{\mu}}_2) \cdot \left[\hat{\boldsymbol{T}}^{(k,\text{ex})}(\boldsymbol{k}_1, \boldsymbol{k}_2, \hat{\boldsymbol{\mu}}_1, \hat{\boldsymbol{\mu}}_2) \right]^{\star} \right], \tag{A2}$$

where we recall that function $\boldsymbol{T}^{(k,\mathrm{ex})}$ is the (reciprocal) dipolar Ewald interaction between two unit dipoles (this interaction corresponds to the dipolar interaction of dipole 2 with dipole 1 and with all the periodic images of dipole 1), and that $\boldsymbol{T}^{(k)}(\boldsymbol{r}_1, \boldsymbol{r}_2, \hat{\boldsymbol{\mu}}_1, \hat{\boldsymbol{\mu}}_2)$ is the corresponding interaction as computed with the P^{3}M algorithm. Equation (A2) involves the Fourier transforms of these functions over $\boldsymbol{r}_1$ and $\boldsymbol{r}_2$.

Using Eqs. (16)–(23), it is possible to show for the non-interlaced case that the electrostatic field generated by a single particle $(\boldsymbol{r}_1, \boldsymbol{\mu}_1)$ acting on a dipole $\boldsymbol{\mu}_2$ at position $\boldsymbol{r}_2$ $\boldsymbol{E}^{(k)}(\boldsymbol{r}_1, \boldsymbol{r}_2, \hat{\boldsymbol{\mu}}_1, \hat{\boldsymbol{\mu}}_2)$ is

$$\boldsymbol{E}^{(k)}(\boldsymbol{r}_1, \boldsymbol{r}_2, \hat{\boldsymbol{\mu}}_1, \hat{\boldsymbol{\mu}}_2) = -\frac{1}{L^3} \sum_{\boldsymbol{r}'_m \in \mathbb{M}^3} \nabla_{\boldsymbol{r}_2} W(\boldsymbol{r}_2 - \boldsymbol{r}'_m) \times \sum_{\boldsymbol{k}_m \in \widetilde{\mathbb{M}}^3} e^{i\boldsymbol{k}_m \cdot \boldsymbol{r}'_m} \widetilde{G}(\boldsymbol{k}_m) \sum_{\boldsymbol{r}_m \in \mathbb{M}^3} e^{-i\boldsymbol{k}_m \cdot \boldsymbol{r}_m} \hat{\boldsymbol{\mu}}_1 \cdot \nabla_{\boldsymbol{r}_1} W(\boldsymbol{r}_1 - \boldsymbol{r}_m)). \tag{A3}$$

Thus, the force and torque acting on the second particle and the interaction energy of particle 2 with particle 1 are

$$\boldsymbol{F}^{(k)}(\boldsymbol{r}_1, \boldsymbol{r}_2, \hat{\boldsymbol{\mu}}_1, \hat{\boldsymbol{\mu}}_2) = (\hat{\boldsymbol{\mu}}_2 \cdot \nabla_{\boldsymbol{r}_2}) \boldsymbol{E}^{(k)} = \nabla_{\boldsymbol{r}_2} (\hat{\boldsymbol{\mu}}_2 \cdot \boldsymbol{E}^{(k)}), \tag{A4}$$

$$\boldsymbol{\tau}^{(k)}(\boldsymbol{r}_1, \boldsymbol{r}_2, \hat{\boldsymbol{\mu}}_1, \hat{\boldsymbol{\mu}}_2) = \hat{\boldsymbol{\mu}}_2 \times \boldsymbol{E}^{(k)}(\boldsymbol{r}_1, \boldsymbol{r}_2, \hat{\boldsymbol{\mu}}_1, \hat{\boldsymbol{\mu}}_2), \tag{A5}$$

$$U^{(k)}(\boldsymbol{r}_1, \boldsymbol{r}_2, \hat{\boldsymbol{\mu}}_1, \hat{\boldsymbol{\mu}}_2) = -\hat{\boldsymbol{\mu}}_2 \cdot \boldsymbol{E}^{(k)}(\boldsymbol{r}_1, \boldsymbol{r}_2, \hat{\boldsymbol{\mu}}_1, \hat{\boldsymbol{\mu}}_2). \tag{A6}$$

The Fourier harmonics $\hat{\boldsymbol{T}}^{(k)}(\boldsymbol{k}_1, \boldsymbol{k}_2, \hat{\boldsymbol{\mu}}_1, \hat{\boldsymbol{\mu}}_2)$ for the reciprocal forces, torques, and energy are obtained by developing Eqs. (A4)–(A6) in Fourier series. For the interlaced version, the use of Eq. (2) implies that the transformed quantity can be obtained as

$$\hat{\boldsymbol{T}}^{(\mathrm{interlaced})}(\boldsymbol{k}_1, \boldsymbol{k}_2) = \hat{\boldsymbol{T}}(\boldsymbol{k}_1, \boldsymbol{k}_2) \frac{1 + \exp(i(\boldsymbol{k}_1 + \boldsymbol{k}_2) \cdot \boldsymbol{p})}{2}. \tag{A7}$$

Thus, the reciprocal expressions used to evaluate the theoretical error estimates for both interlaced and non-interlaced cases are

$$\hat{\boldsymbol{E}}^{(k)}(\boldsymbol{k}_1, \boldsymbol{k}_2) = V(\hat{\boldsymbol{\mu}}_1 \cdot \boldsymbol{k}_1) \breve{U}(\boldsymbol{k}_1) \widetilde{G}(\boldsymbol{k}_1) \times \sum_{\boldsymbol{m} \in \mathbb{Z}^3} \breve{U}(\boldsymbol{k}_{1m}) \boldsymbol{k}_{1m} C(m) \delta_{\boldsymbol{k}_1 + \boldsymbol{k}_2, 2\pi \boldsymbol{m}/h}, \tag{A8}$$

$$\hat{\boldsymbol{\tau}}^{(k)}(\boldsymbol{k}_1, \boldsymbol{k}_2) = \hat{\boldsymbol{\mu}}_2 \times \hat{\boldsymbol{E}}^{(k)}(\boldsymbol{k}_1, \boldsymbol{k}_2), \tag{A9}$$

$$\hat{U}^{(k)}(\boldsymbol{k}_1, \boldsymbol{k}_2) = -\hat{\boldsymbol{\mu}}_2 \cdot \hat{\boldsymbol{E}}^{(k)}(\boldsymbol{k}_1, \boldsymbol{k}_2), \tag{A10}$$

$$\hat{\boldsymbol{F}}^{(k)}(\boldsymbol{k}_1, \boldsymbol{k}_2) = -iV(\hat{\boldsymbol{\mu}}_1 \cdot \boldsymbol{k}_1) \breve{U}(\boldsymbol{k}_1) \widetilde{G}(\boldsymbol{k}_1) \times \sum_{m \in \mathbb{Z}^3} \breve{U}(\boldsymbol{k}_{1m}) (\hat{\boldsymbol{\mu}}_1 \cdot \boldsymbol{k}_{1m}) C(\boldsymbol{m}) \delta_{\boldsymbol{k}_1 + \boldsymbol{k}_2, 2\pi \boldsymbol{m}/h}, \tag{A11}$$

where $\boldsymbol{k}_{1m} = \boldsymbol{k}_1 + 2\pi/h\boldsymbol{m}$. The previous expressions can easily be obtained by recalling the symmetries $\breve{U}(-\boldsymbol{k}) = \breve{U}(\boldsymbol{k})$, $\widetilde{G}(\boldsymbol{k}) = \widetilde{G}(\boldsymbol{k} + 2\pi/h\boldsymbol{m})$, the Fourier series properties such as the shift theorem and the differentiation theorem, as well as the identity:[38]

$$\sum_{\boldsymbol{r}_m \in \mathbb{M}^3} e^{-i\boldsymbol{r}_m \cdot (\boldsymbol{k} - \boldsymbol{k}_m)} = \frac{L^3}{h^3} \sum_{\boldsymbol{n} \in \mathbb{Z}^3} \delta_{\boldsymbol{k}, \boldsymbol{k}_m + \frac{2\pi}{h}\boldsymbol{n}}, \tag{A12}$$

where $\boldsymbol{k} \in \widetilde{\mathbb{K}}^3$.

Once the functions $\hat{\boldsymbol{T}}$ are known, the next step involves the calculus of the exact functions $\hat{\boldsymbol{T}}^{(\mathrm{ex})}$ for the same system. It is straightforward to show that in the case of a system containing two particles the exact functions are

$$\hat{F}^{(k)}(\boldsymbol{k}_1, \boldsymbol{k}_2, \hat{\boldsymbol{\mu}}_1, \hat{\boldsymbol{\mu}}_2) = L^3 \sum_{\substack{\boldsymbol{k} \in \widetilde{\mathbb{K}}^3 \\ \boldsymbol{k} \neq 0}} (\hat{\boldsymbol{\mu}}_2 \cdot i\boldsymbol{k})(\hat{\boldsymbol{\mu}}_1 \cdot i\boldsymbol{k}) i\boldsymbol{k} \breve{\phi}(\boldsymbol{k}) \delta_{\boldsymbol{k}, \boldsymbol{k}_1} \delta_{\boldsymbol{k}, \boldsymbol{k}_2}, \tag{A13}$$

$$\hat{\boldsymbol{\tau}}^{(k)}(\boldsymbol{k}_1, \boldsymbol{k}_2, \hat{\boldsymbol{\mu}}_1, \hat{\boldsymbol{\mu}}_2) = L^3 \sum_{\substack{\boldsymbol{k} \in \widetilde{\mathbb{K}}^3 \\ \boldsymbol{k} \neq 0}} (\hat{\boldsymbol{\mu}}_2 \times i\boldsymbol{k})(\hat{\boldsymbol{\mu}}_1 \cdot i\boldsymbol{k}) \breve{\phi}(\boldsymbol{k}) \delta_{\boldsymbol{k}, \boldsymbol{k}_1} \delta_{\boldsymbol{k}, \boldsymbol{k}_2}, \tag{A14}$$

$$\hat{U}^{(k)}(\boldsymbol{k}_1, \boldsymbol{k}_2, \hat{\boldsymbol{\mu}}_1, \hat{\boldsymbol{\mu}}_2) = -\sum_{\substack{\boldsymbol{k} \in \widetilde{\mathbb{K}}^3 \\ \boldsymbol{k} \neq 0}} (\hat{\boldsymbol{\mu}}_2 \cdot i\boldsymbol{k})(\hat{\boldsymbol{\mu}}_1 \cdot i\boldsymbol{k}) \breve{\phi}(\boldsymbol{k}) \delta_{\boldsymbol{k}, \boldsymbol{k}_1} \delta_{\boldsymbol{k}, \boldsymbol{k}_2}, \tag{A15}$$

where $\delta_{\boldsymbol{k}, \boldsymbol{k}_1}$ and $\delta_{\boldsymbol{k}, \boldsymbol{k}_2}$ are the Kronecker deltas.

Once the values of $\hat{\boldsymbol{T}}$ and $\hat{\boldsymbol{T}}^{(\mathrm{ex})}$ are known, it is possible to simplify the expression (A2) and arrive at the following expression for the rms error of the reciprocal-space components:

$$Q^2_{\mathrm{int}}[\boldsymbol{T}^{(k)}] = \frac{a\boldsymbol{\mu}_1^2 \boldsymbol{\mu}_2^2}{9V^2} \times \sum_{\substack{\boldsymbol{k} \in \widetilde{\mathbb{M}}^3 \\ \boldsymbol{k} \neq 0}} \left[\widetilde{G}^2(\boldsymbol{k}) \left(\sum_{\boldsymbol{m} \in \mathbb{Z}^3} \boldsymbol{k}_{\boldsymbol{m}}^{S_2} \breve{U}^2(\boldsymbol{k}_{\boldsymbol{m}}) \times \sum_{n \in \mathbb{Z}^3} \boldsymbol{k}_{\boldsymbol{mn}}^{S_3} \breve{U}^2(\boldsymbol{k}_{\boldsymbol{mn}}) C(\boldsymbol{n}) \right) + \sum_{m \in \mathbb{Z}^3} |\boldsymbol{k}_{\boldsymbol{m}}|^{2S_1} (\breve{\phi}(\boldsymbol{k}_{\boldsymbol{m}}))^2 - 2\widetilde{G}(\boldsymbol{k}) \times \sum_{m \in \mathbb{Z}^3} \boldsymbol{k}_{\boldsymbol{m}}^{2S_1} \breve{U}^2(\boldsymbol{k}_{\boldsymbol{m}}) \breve{\phi}(\boldsymbol{k}_{\boldsymbol{m}}) \right]. \tag{A16}$$

The set of parameters ($S_1 = 3$, $S_2 = 2$, $S_3 = 4$, $a = 1$) leads to the measure of the error in forces, the set ($S_1 = S_2 = S_3 = 2$, $a = 2$) corresponds to the case of torques, and the set ($S_1 = S_2 = S_3 = 2$, $a = 1$) must be used for the energy. The short-hand notation $\boldsymbol{k}_{\boldsymbol{mn}} \equiv \boldsymbol{k} + 2\pi/h(\boldsymbol{m} + \boldsymbol{n})$ is used in previous expressions.

The optimal influence functions for the different dipolar quantities (force, torque, and energy) can now be obtained by minimizing Eq. (A16) with respect to $\widetilde{G}$,

$$\left. \frac{\delta Q^2_{\mathrm{int}}[\boldsymbol{T}]}{\delta \widetilde{G}} \right|_{\widetilde{G}_{\mathrm{opt}}} = 0. \tag{A17}$$

The optimal influence function expressions obtained are summarized in Eq. (25). Notice that the influence function optimized for torques is the same as for the energy, which is a consequence that for both cases it is necessary to optimize the dipolar electrostatic field since that the dipolar energy for a particle is $U_d = -\boldsymbol{\mu} \cdot \boldsymbol{E}$, and its torque is $\boldsymbol{\tau} = \boldsymbol{\mu} \times \boldsymbol{E}$.

Finally, the expressions for interactions among two particles (Eqs. (A9) and (A11)) allow to compute easily the Madelung-Self interactions by just applying the inverse Fourier series, and taking the limit in which both particles have the same position and dipole, i.e., for a given observable **T**, the Madelung-Self part can be obtained as

$$\mathbf{T}_{\mathrm{MS}}(\boldsymbol{r}, \boldsymbol{\mu}) = \lim_{\substack{r_1, r_2 \to r \\ \mu_1, \mu_2 \to \mu}} \mathrm{FT}^{-1}[\hat{\mathbf{T}}(\boldsymbol{k}_1, \boldsymbol{k}_2, \boldsymbol{\mu}_1, \boldsymbol{\mu}_2)](\boldsymbol{r}_1, \boldsymbol{r}_2, \boldsymbol{\mu}_1, \boldsymbol{\mu}_2). \tag{A18}$$

[1] S. Odenbach, *Magnetoviscous Effects in Ferrofluids*, Lecture Notes in Physics Vol. 71 (Springer, Berlin, 2002).
[2] R. E. Rosensweig, *Ferrohydrodynamics* (Cambridge University Press, Cambridge, 1985).
[3] B. M. Berkovsky, V. F. Medvedev, and M. S. Krakov, *Magnetic Fluids, Engineering, Applications* (Oxford University Press, New York, 1993).
[4] *Magnetic Fluids and Applications Handbook*, edited by B. M. Berkovsky (Begell House Inc., New York, 1996).
[5] C. Holm and J.-J. Weis, Curr. Opin. Colloid Interface Sci. **10**, 133 (2005).
[6] J.-J. Weis and D. Levesque, Adv. Polym. Sci. **185**, 163 (2005).
[7] T. N. Heinz and P. H. Hünenberger, J. Chem. Phys. **123**, 034107 (2005).
[8] M. P. Allen and D. J. Tildesley, *Computer Simulation of Liquids*, 1st ed. (Clarendon, Oxford, 1987).
[9] Z. W. Wang and C. Holm, J. Chem. Phys. **115**, 6277 (2001).
[10] A. Toukmaji, C. Sagui, J. Board, and T. Darden, J. Chem. Phys. **113**, 10913 (2000).
[11] J. J. Cerdà, V. Ballenegger, O. Lenz, and C. Holm, J. Chem. Phys. **129**, 234104 (2008).
[12] R. Kutteh and J. B. Nicholas, Comput. Phys. Commun. **86**, 236 (1995).
[13] R. Kutteh and J. B. Nicholas, Comput. Phys. Commun. **86**, 227 (1995).
[14] A. D. Stoycheva and S. J. Singer, Phys. Rev. E **65**, 036706 (2002).
[15] D. Christiansen, J. W. Perram, and H. G. Petersen, J. Comput. Phys. **107**, 403 (1993).
[16] A. Arnold and C. Holm, "Efficient methods to compute long range interactions for soft matter systems," in *Advanced Computer Simulation Approaches for Soft Matter Sciences II*, Advances in Polymer Sciences Vol II, edited by C. Holm and K. Kremer (Springer, Berlin, 2005), pp. 59–109.
[17] H. G. Petersen, J. Chem. Phys. **103**, 3668 (1995).
[18] C. Sagui and T. A. Darden, AIP Conf. Proc. **492**, 104 (1999).
[19] M. Deserno and C. Holm, J. Chem. Phys. **109**, 7678 (1998).
[20] V. Ballenegger, J. J. Cerda, and C. Holm, "How to convert SPME to P^{3}M: influence function and error estimates," J. Chem. Phys. (submitted).
[21] J. W. Eastwood, J. Comput. Phys. **18**, 1 (1975).
[22] A. B. Langdon, J. Comput. Phys. **12**, 247 (1973).
[23] U. Essmann, L. Perera, M. L. Berkowitz, T. Darden, H. Lee, and L. G. Pedersen, J. Chem. Phys. **103**, 8577 (1995).
[24] R. W. Hockney and J. W. Eastwood, *Computer Simulations using Particles* (McGraw-Hill, New York, 1981).
[25] V. Ballenegger, J. J. Cerda, and C. Holm, Comput. Phys. Commun. **182**, 1919 (2011).
[26] C. B. L. Chen, A. B. Langdon, J. Comput. Phys. **14**, 200 (1974).
[27] D. S. Cerutti, R. E. Duke, T. A. Darden, and T. P. Lybrand, J. Chem. Theory Comput. **5**, 2322 (2009).
[28] A. Neelov and C. Holm, J. Chem. Phys. **132**, 234103 (2010).
[29] P. Ewald, Ann. Phys. **369**, 253 (1921).
[30] G. Rajagopal and R. Needs, J. Comput. Phys. **115**, 399 (1994).
[31] P. H. Hünenberger, J. Chem. Phys. **113**, 10464 (2000).
[32] P. F. Batcho and T. Schlick, J. Chem. Phys. **115**, 8312 (2001).
[33] D. Frenkel, Science **296**, 65 (2002).
[34] S. W. de Leeuw, J. W. Perram, and E. R. Smith, Proc. R. Soc. London, Ser. A **373**, 27 (1980).
[35] S. W. de Leeuw, J. W. Perram, and E. R. Smith, Proc. R. Soc. London, Ser. A **373**, 57 (1980).
[36] J. W. Eastwood, "Optimal P^{3}M algorithms for molecular dynamcis simulations," in *Computational Methods in Classical and Quantum Physics* (Advace Publications Limited, London, 1976).
[37] M. Frigo and S. G. Johnson, Proc. IEEE **93**, 216 (2005) (Special issue on "Program Generation, Optimization, and Platform Adaptation").
[38] H. A. Stern and K. G. Calkins, J. Chem. Phys. **128**, 214106 (2008).